Separation Science and Technology
Publication details, including instructions for authors and subscription information:
http://www.informaworld.com/smpp/title~content=t713708471

Nonequilibrium Theory for Field-Flow Fractionation in Annular Channels

Joe M. Davis[a]
[a] DEPARTMENT OF CHEMISTRY AND BIOCHEMISTRY, SOUTHERN ILLINOIS UNIVERSITY CARBONDALE, ILLINOIS

To cite this Article Davis, Joe M.(1989) 'Nonequilibrium Theory for Field-Flow Fractionation in Annular Channels', Separation Science and Technology, 24: 3, 219 — 245
To link to this Article: DOI: 10.1080/01496398908049764
URL: http://dx.doi.org/10.1080/01496398908049764

SEPARATION SCIENCE AND TECHNOLOGY, 24(3&4), pp. 219-245, 1989

Nonequilibrium Theory for Field-Flow Fractionation in Annular Channels

JOE M. DAVIS

DEPARTMENT OF CHEMISTRY AND BIOCHEMISTRY
SOUTHERN ILLINOIS UNIVERSITY
CARBONDALE, ILLINOIS 62901

Abstract

The principles of field-flow fractionation (FFF) and reasons for extending the FFF methodology from parallel-plate channels to annular channels (ANNCs) are briefly reviewed. A theory for the nonequilibrium plate height H of FFF zones in ANNCs is developed by extending the nonequilibrium theory of FFF to polar coordinates. The principal assumption in the theory is that component zones are localized near the ANNC walls by the general force $F = A/r^n$, where A and n are constants and r is the radial coordinate. Equations for H are developed as functions of n, the inner-to-outer radius ratio of the ANNC, and the fundamental FFF parameter, λ. A closed-form analytical solution to H is obtained when $n = 1$; the $n \neq 1$ solution must generally be expressed as a ratio of the integrals involved. These integrals can be approximated analytically, however, when $\lambda \ll 1$. The functions for H are compared to their parallel-plate counterpart, and differences are rationalized.

INTRODUCTION

Field-flow fractionation (FFF) is a family of chromatographic-like separation methods well adapted to the separation and analytical characterization of macromolecules, colloids, emulsions, viruses, proteins, cells, and similar species. The principles of FFF are detailed elsewhere (*1*, *2*) and are only briefly reviewed here. Separation by FFF is effected by the differential transport by laminar flow of sample components through an open channel of thin lateral dimensions, as shown in Fig. 1. Each sample component is localized or concentrated into a zone

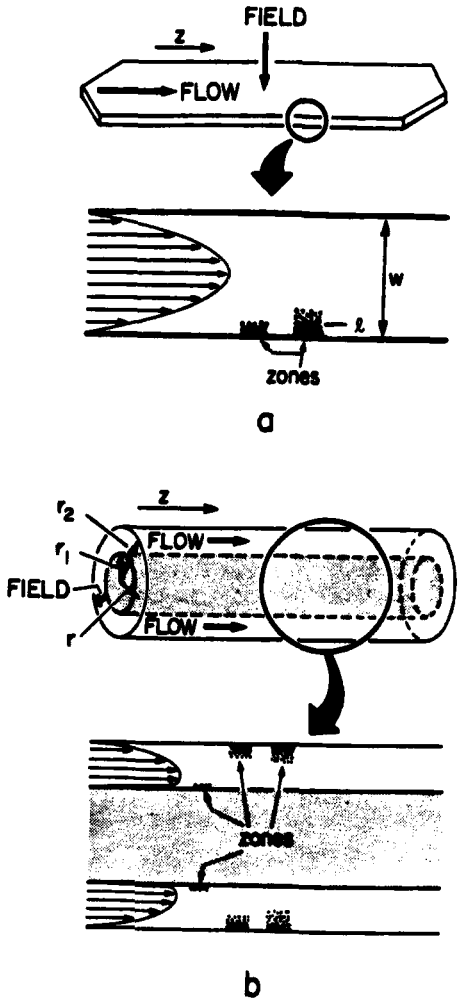

FIG. 1. (a) Open parallel-plate channel (OPPC) traditionally used in FFF. (b) Annular channel (ANNC). Reprinted with permission from Ref. 9, copyright 1985 American Chemical Society.

of characteristic thickness near one channel wall (the accumulation wall) by a field or gradient which is perpendicular to the flow direction. The more localized components (zones) are carried by flow through the channel more slowly than less localized components because the flow approaches zero at the channel walls.

The mathematical descriptions of fields (gradients) and laminar flow in FFF systems are usually fairly simple. This simplicity has facilitated the derivation from theory of fairly rigorous expressions for the behavior of component zones in FFF channels. Of particular importance are the equations that describe the relative rate of zone migration through the channel, as expressed by the retention ratio, and the dispersion of zone constituents along the flow coordinate, as expressed by the plate height. These equations depend on (among other things) the field strength, channel width, temperature, flow rate, and various physicochemical properties of the sample components. By fitting these equations to experimental measurements of the corresponding behavior, one can estimate these properties from theory, and thus use FFF as a tool for analytical characterization.

The majority of FFF has been implemented with rectangular open parallel-plate channels (OPPCs) of the type shown in Fig. 1(a). A small number of experiments, however, have been carried out in circular (*3–7*) and annular (*8*) channels. The annular channel (ANNC) shown in Fig. 1(b) is a particularly attractive alternative to the OPPC, because several mathematically well-defined fields, e.g., shear, dielectrophoretic, and magnetophoretic, can be more easily generated in ANNCs than in OPPCs. The utilization of these fields with ANNCs would extend the FFF methodology to new sample properties and types. Other fields, e.g., thermal, flow, electrical, and sedimentation, can be generated in both OPPCs and ANNCs, with one channel type perhaps accruing slight advantages over the other in specific cases (*9*).

A proper evaluation of the relative merits of OPPCs, ANNCs, and circular channels as conduits for FFF must include a judicious comparison of the retention ratio and plate height. The latter attribute is a sum of several independent terms, the largest (and most important) of which is usually the nonequilibrium contribution. Theories were developed some years ago for the retention ratio and nonequilibrium plate height of zones in OPPCs (*10, 11*) and circular channels (*4, 12*) immersed in uniform, unidirectional fields. A theory for the retention ratio of zones in ANNCs was recently developed, and it addressed the retardation of zone migration rates by a radial field (*9*). A complementary theory that quantifies the principal source of zone dispersion in ANNCs is presented

below. This work entails a derivation by nonequilibrium theory of the nonequilibrium plate height of FFF zones in ANNCs immersed in a radial field.

THEORY

The origin of nonequilibrium dispersion is the differential transport by flow of a zone's constituent members: zone members in fast streamlines move ahead of those in slow streamlines. The result is a broadening of the zone along the flow coordinate. The broadening is mitigated by the diffusive exchange of zone members among streamlines of different velocity. The relative magnitude of this dispersion is commonly expressed in elutive methods, including FFF, as the nonequilibrium plate height, $H = \sigma^2/L$. Here, σ^2 is that fraction of the total zone variance, which has many origins, that arises from differential flow, and L is the average distance the zone is carried by flow.

The nonequilibrium plate height, H_p, of zones in OPPCs, as derived from nonequilibrium theory, is (*11*, *13*)

$$H_p = \Psi_p \ell^2 \nu / D = \chi_p w^2 \langle V_z \rangle / D = 24\lambda^3 f(\lambda) w^2 \langle V_z \rangle / D \qquad (1)$$

where ℓ is the characteristic zone thickness and w is the width of the OPPC, as shown in Fig. 1(a), $\lambda = \ell/w = kT/F_p w$, $\langle V_z \rangle$ and ν are the average linear velocities of the carrier fluid (or simply carrier) and zone, F_p is the uniform force that localizes the zone near the accumulation wall, and D is the constant diffusion coefficient of the component (zone). The quantity λ, the fundamental parameter in FFF theory, is also defined by

$$\lambda = kT/|W| \qquad (2)$$

where kT is the average thermal energy of the carrier and $|W|$ is the magnitude of work W done by the force F_p in moving zone constituents across gap w. The factors Ψ_p and χ_p are complicated functions of λ defined elsewhere (*11*) and are related by the expression $\chi_p = \Psi_p \lambda^2 R_p$, where

$$R_p = \nu/\langle V_z \rangle = 6\lambda\left(\coth\left(\frac{1}{2\lambda}\right) - 2\lambda\right) = 6\lambda g(\lambda) \qquad (3)$$

is the expression for the retention ratio in OPPCs (*10*). The functions $f(\lambda)$ and $g(\lambda)$ both approach 1 as λ approaches zero.

The nonequilibrium theory for ANNCs developed below draws extensively from the theory for retention ratio R in ANNCs. The present treatment is restricted to the case in which each zone is carried by steady laminar flow in the axial direction and is concentrated near the accumulation wall by the time-independent force F:

$$F = A/r^n \tag{4}$$

where r is the radial coordinate (shown in Fig. 1b) and n has any real value. The values of n corresponding to the forces noted in the Introduction, for example, are $n = 5$ (shear), 3 (magnetophoretic and dielectrophoretic), 1 (electrical, flow, and thermal), and -1 (sedimentation). Coefficient A is positive when the zone is concentrated near the outer wall of the ANNC, and negative when the zone is concentrated near the inner wall.

The nonequilibrium plate height H will be calculated from the continuity equation in polar coordinates, which is (*14*)

$$\frac{\partial c}{\partial t} + \frac{1}{r}\frac{\partial}{\partial r}(rN_r) + \frac{\partial N_z}{\partial z} = 0 \tag{5}$$

where c is the component concentration, t is time, z is the axial coordinate parallel to the flow direction (see Fig. 1b), and N_r and N_z are, respectively, the one-dimensional radial and axial fluxes:

$$N_r = V_r c - D\frac{\partial c}{\partial r} \tag{6}$$

$$N_z = V_z c - D\frac{\partial c}{\partial z} \tag{7}$$

No angular flux appears in Eq. (5) because of radial symmetry. In Eq. (6), V_r is the radial velocity of the component (zone) induced by force F and is defined by

$$V_r = F/f = AD/kTr^n \tag{8}$$

where $f = kT/D$ is the friction coefficient. The function V_z in Eq. (7) is the linear velocity of the carrier, which in dimensionless coordinates is

$$V_z = 2\frac{\langle V_z \rangle}{\Phi}(1 - \rho^2 - \theta \ln \rho) = R\langle V_z \rangle \mu \tag{9}$$

where

$$\theta = \frac{1 - \rho_1^2}{\ln \rho_1} \tag{10}$$

and

$$\Phi = 1 + \rho_1^2 + \theta \tag{11}$$

In Eqs. (9)–(11), $\rho = r/r_2$ and $\rho_1 = r_1/r_2$, where r_1 and r_2 are, respectively, the radii of the inner and outer walls of the ANNC, as shown in Fig. 1(b). The function μ is the reduced velocity, V_z/v. The constants $\langle V_z \rangle$ and $v = R\langle V_z \rangle$ are, as before, the average linear velocities of the carrier and zone. The mean linear fluid velocity $\langle V_z \rangle$ was evaluated according to Eq. (12), the general formula for the cross-sectional average of the general function $f(r)$:

$$\langle f(r) \rangle = 2\int_{r_1}^{r_2} rf(r)dr/(r_2^2 - r_1^2) = 2\int_{\rho_1}^{1} \rho f(r_2\rho)d\rho/(1 - \rho_1^2) \tag{12}$$

One obtains, after expanding Eq. (5) by Eqs. (6) and (7) and equating $\partial V_z/\partial z$ to zero, because the flow is steady, the following expression for the continuity equation:

$$\frac{\partial c}{\partial t} + \frac{V_r c}{r} + c\frac{\partial V_r}{\partial r} + V_r\frac{\partial c}{\partial r} + V_z\frac{\partial c}{\partial z} = D\left(\frac{\partial^2 c}{\partial r^2} + \frac{1}{r}\frac{\partial c}{\partial r} + \frac{\partial^2 c}{\partial z^2}\right) \tag{13}$$

A minimal outline of nonequilibrium theory, as developed by Giddings, is presented here because (for reasons given below) two derivations of H are required to characterize ANNCs, and this outline will minimize redundancy. Specific details of the theory are best sought in Giddings' extensive applications of it to chromatography (*15*) and FFF in OPPCs (*11*, *13*, *16*). In brief, Eq. (13) will be simplified to an ordinary second-order differential equation by several approximations. From the solution to this differential equation and other functions, a flow-induced effective diffusion coefficient will be determined by the method reported by Giddings (*13*). This effective diffusion coefficient is a measure of the dispersion of zone constituents along the flow coordinate, i.e., the nonequilibrium broadening. From this effective diffusion coefficient, the plate height will be calculated.

Because the mathematical form of the one-dimensional flux N_z is

identical in both Cartesian and polar coordinates, many of the equations developed for OPPCs also apply to ANNCs. In particular, the near-equilibrium approximation (*13*)

$$\frac{\partial c}{\partial t} \approx D \frac{\partial^2 c^*}{\partial z^2} - v \frac{\partial c^*}{\partial z} \tag{14}$$

is still valid, provided that $v = R\langle V_z \rangle$ is calculated in accordance with Eq. (12). The concentration c can also be expanded as a truncated power series about the quasi-equilibrium concentration c^* (*13*):

$$c = c^*(1 + \varepsilon) \tag{15}$$

where $\varepsilon = \varepsilon(r,z)$ is the fractional departure of c from c^*. (One determines the concentration c^* by solving the differential equation $N_r^* = 0$, where N_r^* equals Eq. 6 with c replaced by c^*; the derivation is given in Ref. *9*.) The substitution of Eqs. (14) and (15) into Eq. (13) results in a second-order differential equation for the function ε.

By substituting Eq. (15) into Eq. (7), expanding, and interpreting the resultant terms, Giddings showed, by using Fick's first law in Cartesian coordinates, that the flow-induced effective diffusion coefficient, **D**, is (*13*)

$$\mathbf{D} = -\frac{\langle c^* V_z \varepsilon \rangle}{\langle c^* \rangle \partial \ln c^* / \partial z} \tag{16}$$

The plate height $H = \sigma^2/L$ was then calculated from Eq. (16) and the Einstein diffusion equation, $\sigma^2 = 2\mathbf{D}t = 2\mathbf{D}L/v$, as (*13*)

$$H = 2\mathbf{D}/v \tag{17}$$

Thus, a solution to the differential equation for ε is required to determine H from Eqs. (16) and (17). These equations also apply to ANNCs, provided that cross-sectional averages are calculated in accordance with Eq. (12).

Two boundary conditions are needed to determine a unique solution to the differential equation; three possible boundary conditions exist. Two of them may be expressed as

$$\left.\frac{\partial \varepsilon}{\partial r}\right|_{r_1,r_2} = \left.\frac{\partial \phi}{\partial \rho}\right|_{\rho_1,1} = 0 \tag{18}$$

where the function ϕ is defined below, and the third as

$$\langle c^*\varepsilon \rangle = 0 \tag{19}$$

Equation (18) states that no radial flux crosses either ANNC wall and is derived by substituting Eq. (15) into $N_r^* = 0$ (*13*). Equation (19) states that mass is conserved along the radial coordinate, i.e., that $\langle c \rangle = \langle c^* \rangle$ (*13*).

Some alternative definitions of H, derived from the above equations, will be useful for later comparisons of H to H_p, Eq. (1). By introducing the function [similar to one previously defined for OPPC systems (*13*)]

$$\phi = \frac{\varepsilon D}{\nu r_2^2 \partial \ln c^*/\partial z} \tag{20}$$

one may express H as

$$H = -2\frac{\langle c^*\mu\phi \rangle}{\langle c^* \rangle}\frac{r_2^2\nu}{D} = -2\frac{\langle c^*(\mu - 1)(\phi - g_1) \rangle}{\langle c^* \rangle}\frac{r_2^2\nu}{D} \tag{21}$$

$$= \frac{\Psi r_2^2 \nu}{D} = \frac{\Psi R}{(1 - \rho_1)^2}\frac{w^2\langle V_z \rangle}{D} = \frac{\chi w^2 \langle V_z \rangle}{D} \tag{22}$$

where

$$\Psi = -2\langle c^*(\mu - 1)(\phi - g_1) \rangle / \langle c^* \rangle \tag{23}$$

and

$$\chi = \Psi R/(1 - \rho_1)^2 \tag{24}$$

The identity of the bracketed expressions in the numerators of Eq. (21) follows from Eq. (19) and the definitions of μ, the reduced velocity (Eq. 9), and $\nu = \langle c^* V_z \rangle / \langle c^* \rangle$. The quantity g_1 is a constant of integration. The width w of the gap between the inner and outer ANNC walls has been defined in Eq. (22) as $w = r_2 - r_1 = r_2(1 - \rho_1)$, for later comparison to Eq. (1). The function ϕ, Eq. (20), will be useful below.

Two solutions to concentration c^* and retention ratio R exist, corresponding to the cases where $n = 1$ and $n \neq 1$ in Eq. (4) (*9*). Because H depends on both functions, two solutions to H also exist, corresponding to the same cases. The case for $n \neq 1$ is treated first.

CASE ONE: $n \neq 1$

The dimensionless concentration c^* for this case is (9)

$$c^* = K_1 \exp(\mp \alpha \rho^{1-n}) \tag{25}$$

where K_1 is a constant. The parameter α is

$$\alpha = \frac{1}{\lambda(\rho_1^{1-n} - 1)} \tag{26}$$

where

$$\lambda = \frac{kT}{|W|} = \frac{kT}{\int_{r_1}^{r_2} \frac{|A|}{r^n} dr} = \frac{(1-n)kT}{|A| r_2^{1-n}(1 - \rho_1^{1-n})} \tag{27}$$

The upper and lower signs that multiply the exponential factor of Eq. (25) indicate that c^* differs for inner-wall and outer-wall retention. The upper sign (in this case, negative) applies when the zone forms near the outer wall of the ANNC, and the lower sign applies when the zone forms near the inner wall.

The first step is to express the continuity equation in terms of c^*. Using Eqs. (26) and (27), one can express velocity V_r, Eq. (8), as

$$V_r = \pm \frac{(n-1)\alpha D}{\rho^n r_2} \tag{28}$$

The derivatives $\partial c^*/\partial r$ and $\partial V_r/\partial r$ are calculated as

$$\frac{\partial c^*}{\partial r} = \frac{\partial c^*}{\partial \rho} \frac{\partial \rho}{\partial r} = \pm \frac{(n-1)\alpha}{\rho^n r_2} c^* \tag{29}$$

$$\frac{\partial V_r}{\partial r} = \frac{\partial V_r}{\partial \rho} \frac{\partial \rho}{\partial r} = \mp \frac{n(n-1)\alpha D}{\rho^{n+1} r_2^2} \tag{30}$$

where $\partial \rho/\partial r = r_2^{-1}$. By combining Eqs. (15) and (28)–(30), one can show that the various terms comprising Eq. (13) equal

$$\frac{V_r c}{r} = \pm \frac{(n-1)\alpha D}{\rho^{n+1}} (1 + \varepsilon) \frac{c^*}{r_2^2} \tag{31}$$

$$c\frac{\partial V_r}{\partial r} = \mp\frac{n(n-1)\alpha D(1+\varepsilon)}{\rho^{n+1}}\frac{c^*}{r_2^2} \tag{32}$$

$$V_r\frac{\partial c}{\partial r} = \frac{(n-1)\alpha D}{\rho^n}\left(\frac{(n-1)\alpha}{\rho^n}(1+\varepsilon) \pm \frac{\partial \varepsilon}{\partial \rho}\right)\frac{c^*}{r_2^2} \tag{33}$$

$$\frac{\partial^2 c}{\partial r^2} = \left[\frac{(n-1)\alpha}{\rho^n}\left\{\left(\frac{(n-1)\alpha}{\rho^n} \mp \frac{n}{\rho}\right)(1+\varepsilon) \pm 2\frac{\partial \varepsilon}{\partial \rho}\right\} + \frac{\partial^2 \varepsilon}{\partial \rho^2}\right]\frac{c^*}{r_2^2} \tag{34}$$

$$\frac{1}{r}\frac{\partial c}{\partial r} = \left\{\frac{1}{\rho}\frac{\partial \varepsilon}{\partial \rho} \pm \frac{(n-1)\alpha}{\rho^{n+1}}(1+\varepsilon)\right\}\frac{c^*}{r_2^2} \tag{35}$$

$$V_z\frac{\partial c}{\partial z} \approx V_z\frac{\partial c^*}{\partial z} \tag{36}$$

$$\frac{\partial^2 c}{\partial z^2} \approx \frac{\partial^2 c^*}{\partial z^2} \tag{37}$$

Equations (36) and (37) are approximations based on the inequality $\partial\varepsilon/\partial z \ll \partial\varepsilon/\partial r$, which applies because the zone's radial dimension is much smaller than its axial dimension. A similar approximation was used to derive H_p for zones in OPPCs (*13*).

Combining Eqs. (14) and (31)-(37) with Eq. (13), one derives the following differential equation for ε:

$$r_2^2\frac{V_z - v}{D}\frac{\partial \ln c^*}{\partial z} = \frac{\partial^2 \varepsilon}{\partial \rho^2} + \left(\frac{1}{\rho} \pm \frac{(n-1)\alpha}{\rho^n}\right)\frac{\partial \varepsilon}{\partial \rho} \tag{38}$$

Substituting Eq. (20) into Eq. (38), one obtains the alternative dimensionless form

$$\mu - 1 = \frac{d^2\phi}{d\rho^2} + \left(\frac{1}{\rho} \pm \frac{(n-1)\alpha}{\rho^n}\right)\frac{d\phi}{d\rho} \tag{39}$$

where μ is defined by Eq. (9). The partial derivatives have been replaced by ordinary ones, because the functional dependence of ε and ϕ on z has been neglected.

Equation (39) must now be solved for ϕ. An integrating factor for Eq. (39) is

$$\rho \exp(\mp\alpha\rho^{1-n}) = \rho e^{\mp x} \tag{40}$$

where the function x

$$x = \alpha\rho^{1-n} \tag{41}$$

has been introduced to simplify subsequent equations. The integration of Eq. (39) yields

$$\rho e^{\mp x}\frac{d\phi}{d\rho} = \int_{\delta}^{\rho} \rho e^{\mp x}(\mu - 1)d\rho \tag{42}$$

where the lower integration limit δ can equal ρ_1 or 1, in accordance with the boundary condition, Eq. (18). (The appropriate δ value is addressed below.) The integration of Eq. (42) gives

$$\phi - g_1 = \int_{\delta}^{\rho}\frac{1}{\rho}e^{\pm x}\int_{\delta}^{\rho}\rho e^{\mp x}(\mu - 1)d\rho\, d\rho \tag{43}$$

where the constant g_1 is the value of ϕ at $\rho = \delta$. Combining Eq. (43) with Eq. (23), one determines that the function Ψ for the $n \neq 1$ case is

$$\Psi = -2\frac{\displaystyle\int_{\rho_1}^{1}\rho(\mu - 1)e^{\mp x}\int_{\delta}^{\rho}\frac{e^{\pm x}}{\rho}\int_{\delta}^{\rho}\rho e^{\mp x}(\mu - 1)d\rho\, d\rho\, d\rho}{\displaystyle\int_{\rho_1}^{1}\rho e^{\mp x}d\rho} \tag{44}$$

Integrating Eq. (44) by parts and significantly simplifying the integration by Eq. (18), as detailed in an earlier work (*11*), one determines that

$$\Psi = 2\frac{\displaystyle\int_{\rho_1}^{1}\frac{1}{\rho}e^{\pm x}\left(\int_{\delta}^{\rho}\rho e^{\mp x}(\mu - 1)d\rho\right)^2 d\rho}{\displaystyle\int_{\rho_1}^{1}\rho e^{\pm x}d\rho} \tag{45}$$

By changing the integration variable in Eq. (45) from ρ to x, Eq. (41), one obtains the desired result

$$\Psi = \frac{8}{\{(1-n)\alpha^{1/(1-n)}R\Phi\}^2}\int_{\alpha\rho_1^{1-n}}^{\alpha}\frac{e^{\pm x}}{x}\left\{\int_{\delta'}^{x}x^{(n+1)/(1-n)}e^{\mp x}\right.$$

$$\times \frac{\left(1 - R\Phi/2 - \left(\frac{x}{\alpha}\right)^{2/(1-n)} - \frac{\theta}{(1-n)} \ln\left(\frac{x}{\alpha}\right)\right) dx\Big\}^2 dx}{\int_{\alpha\rho_1^{1-n}}^{\alpha} x^{(n+1)/(1-n)} e^{\mp x}\, dx} \tag{46}$$

where δ' can equal α or $\alpha\rho_1^{1-n}$ and μ has been explicitly expressed.

From a consideration of nonequilibrium theory, both values for δ and δ' given above are possible integration limits for the above equations. Thus, theory does not provide guidelines for the determination of a unique solution to Ψ. It was determined empirically in this study, however, that the limits δ and δ' must be

$$\delta = 1$$
$$\delta' = \alpha \tag{47}$$

when zones are retained at the inner wall, and

$$\delta = \rho_1$$
$$\delta' = \alpha\rho_1^{1-n} \tag{48}$$

when zones are retained at the outer wall. With these (apparently arbitrary) assignments, the function Ψ behaves as expected in the $\lambda \to 0$ limit. If the assignments to δ and δ' are reversed, however (e.g., if $\delta = 1$ and $\delta' = \alpha$ for the outer-wall calculation), then $\Psi \to \infty$, instead of zero as expected, as $\lambda \to 0$.

Equation (46) cannot be evaluated analytically for any n of current interest (e.g., $n = 5$, 3, and -1). Because adequate retention (i.e., $R < 0.5$) will not be attained unless $\lambda \ll 1$ (*9*), the most interesting case of this equation corresponds to $|\alpha| \gg 1$, for which a power-series solution is computationally untractable because of the exponential terms. In general, Eq. (46) is perhaps best evaluated by numerical integration. An alternative approach, based on the rapid variation of the exponential terms in Eq. (46), allows one to derive analytical approximations to this equation when $|\alpha| \gg 1$ ($\lambda \ll 1$). The procedure has been detailed elsewhere (*9*, *17*); only the results of this particular application are given here.

$$\Psi_{in} = \left(\frac{2\rho_1^n}{(n-1)\alpha}\right)^2, \qquad \lambda \ll 1 \tag{49}$$

$$\Psi_{out} = \left(\frac{2}{(n-1)\alpha}\right)^2, \qquad \lambda \ll 1 \tag{50}$$

Here, Ψ_{in} and Ψ_{out} are the asymptotically correct Ψ functions for inner- and outer-wall retention, respectively, that Eq. (46) approaches as $\lambda \to 0$.

The function H can be calculated for the $n \neq 1$ case from the above equations, provided that retention ratio R is known. The expression for R is (*9*)

$$R = \frac{2}{\Phi} \frac{\displaystyle\int_{\alpha\rho_1^{1-n}}^{\alpha} x^{(n+1)/(1-n)} e^{\mp x} \left(1 - \left(\frac{x}{\alpha}\right)^{2/(1-n)} - \frac{\theta}{(1-n)} \ln\left(\frac{x}{\alpha}\right)\right) dx}{\displaystyle\int_{\alpha\rho_1^{1-n}}^{\alpha} x^{(n+1)/(1-n)} e^{\mp x}\, dx} \tag{51}$$

Equation (51) also cannot be generally evaluated analytically for n values of interest, but the ratio of integrals approaches the limits (*9*)

$$R_{in} = -\frac{2\rho_1^{n-1}}{(n-1)\alpha\Phi}(2\rho_1^2 + \theta); \qquad R_{out} = \frac{2}{(n-1)\alpha\Phi}(2 + \theta), \qquad \lambda \ll 1 \tag{52}$$

when $|\alpha| \gg 1$ and $\lambda \ll 1$. Here, R_{in} and R_{out} are the retention ratios for inner- and outer-wall retention, respectively.

Combining Eqs. (24), (49), (50), and (52), one obtains the following limiting expressions for function χ

$$\chi_{in} = \frac{-8\lambda^3\rho_1^2}{\Phi(1-\rho_1)^2}\left(\frac{1-\rho_1^{n-1}}{n-1}\right)^3(2\rho_1^2 + \theta), \qquad \lambda \ll 1 \tag{53}$$

$$\chi_{out} = \frac{8\lambda^3}{\Phi(1-\rho_1)^2}\left(\frac{1-\rho_1^{n-1}}{(n-1)\rho_1^{n-1}}\right)^3(2 + \theta), \qquad \lambda \ll 1 \tag{54}$$

where the subscripts are interpreted as before. As $\rho_1 \to 1$, the ANNC is converted into an OPPC, for which $H = H_p$, Eq. (1). The limit of Eqs. (53) and (54), as $\rho_1 \to 1$, is $24\lambda^3$, in agreement with Eq. (1).

CASE TWO: $n = 1$

This case is treated exactly as before, except the functions c^* and R differ from their $n \neq 1$ counterparts. The dimensionless concentration profile c^* here is (9)

$$c^* = K_2 \rho^{\pm\beta} \tag{55}$$

where K_2 is a constant. As before, the upper sign (in this case, positive) that multiplies the exponent in Eq. (55) applies when the zone forms near the outer ANNC wall, and the lower sign applies when the zone forms near the inner wall. The parameter β is positive and has the value

$$\beta = -(\lambda \ln \rho_1)^{-1} \tag{56}$$

where

$$\lambda = \frac{kT}{|W|} = \frac{kT}{\int_{r_1}^{r_2} \frac{|A|}{r} dr} = -\frac{kT}{|A| \ln \rho_1} \tag{57}$$

As before, the first objective is to express the continuity equation, Eq. (13), in terms of c^*. Using Eqs. (56) and (57), one can express the radial velocity V_r, Eq. (8), as

$$V_r = \pm \frac{\beta D}{\rho r_2} \tag{58}$$

The derivatives $\partial c^*/\partial r$ and $\partial V_r/\partial r$ are

$$\frac{\partial c^*}{\partial r} = \pm \frac{\beta c^*}{\rho r_2} \tag{59}$$

$$\frac{\partial V_r}{\partial r} = \mp \frac{\beta D}{\rho^2 r_2^2} \tag{60}$$

Combining Eqs. (58)–(60) with Eq. (15) and the terms in Eq. (13) that depend on r, one finds that

$$\frac{V_r c}{r} = \pm \frac{\beta D(1 + \varepsilon)}{\rho^2} \frac{c^*}{r_2^2} \tag{61}$$

$$c\frac{\partial V_r}{\partial r} = \mp\frac{\beta D(1+\varepsilon)}{\rho^2}\frac{c^*}{r_2^2} \tag{62}$$

$$V_r\frac{\partial c}{\partial r} = \frac{\beta D}{\rho}\left(\frac{\beta}{\rho}(1+\varepsilon) \pm \frac{\partial \varepsilon}{\partial \rho}\right)\frac{c^*}{r_2^2} \tag{63}$$

$$\frac{\partial^2 c}{\partial r^2} = \left[\frac{\beta}{\rho}\left(\frac{1}{\rho}(\beta \mp 1)(1+\varepsilon) \pm 2\frac{\partial \varepsilon}{\partial \rho}\right) + \frac{\partial^2 \varepsilon}{\partial \rho^2}\right]\frac{c^*}{r_2^2} \tag{64}$$

$$\frac{1}{r}\frac{\partial c}{\partial r} = \frac{1}{\rho}\left(\frac{\partial \varepsilon}{\partial \rho} \pm \frac{\beta}{\rho}(1+\varepsilon)\right)\frac{c^*}{r_2^2} \tag{65}$$

Substituting Eqs. (14), (36), (37), and (61)–(65) into Eq. (13), one determines that the differential equation for ε is

$$r_2^2\frac{V_z - v}{D}\frac{\partial \ln c^*}{\partial z} = \frac{\partial^2 \varepsilon}{\partial \rho^2} + \frac{1 \pm \beta}{\rho}\frac{\partial \varepsilon}{\partial \rho} \tag{66}$$

which becomes, after one substitutes ϕ, Eq. (20), for ε

$$\mu - 1 = \frac{d^2\phi}{d\rho^2} + \frac{1 \pm \beta}{\rho}\frac{d\phi}{d\rho} \tag{67}$$

A comparison of Eqs. (26), (39), (56), and (67) shows that the identity

$$\lim_{n\to 1}\frac{(1-n)\rho^{1-n}}{(\rho_1^{1-n}-1)} = (\ln \rho_1)^{-1} \tag{68}$$

must exist if the differential equations derived for the $n = 1$ and $n \neq 1$ cases are internally consistent. Equation (68) can indeed be confirmed by Taylor-series expansion.

Equation (67) must be solved for ϕ. An integrating factor for Eq. (67) is $\rho^{1\pm\beta}$. The integration of Eq. (67) yields

$$\rho^{1\pm\beta}\frac{d\phi}{d\rho} = \int_\delta^\rho \rho^{1\pm\beta}(\mu - 1)\,d\rho \tag{69}$$

where, as before, δ equals ρ_1 for outer-wall retention and 1 for inner-wall retention. The integration of Eq. (69) gives

$$\phi - g_1 = \int_\delta^\rho \rho^{-(1\pm\beta)} \int_\delta^\rho \rho^{1\pm\beta}(\mu - 1)\, d\rho\, d\rho \tag{70}$$

where, as before, g_1 is the value of ϕ at $\rho = \delta$. Equation (70) is combined with the definition of Ψ, Eq. (23), to give

$$\Psi = -2\frac{\displaystyle\int_{\rho_1}^1 \rho^{1\pm\beta}(\mu - 1) \int_\delta^\rho \rho^{-(1\pm\beta)} \int_\delta^\rho \rho^{1\pm\beta}(\mu - 1)\, d\rho\, d\rho\, d\rho}{\displaystyle\int_{\rho_1}^1 \rho^{1\pm\beta}\, d\rho} \tag{71}$$

A simplification of Eq. (71) by the integration-by-parts procedure previously referenced yields the expression

$$\Psi = 2\frac{\displaystyle\int_{\rho_1}^1 \rho^{-(1\pm\beta)}\left(\int_\delta^\rho \rho^{1\pm\beta}(\mu - 1)\, d\rho\right)^2 d\rho}{\displaystyle\int_{\rho_1}^1 \rho^{1\pm\beta}\, d\rho} \tag{72}$$

Equation (72) can be evaluated analytically. The result is

$$\begin{aligned}\Psi = \frac{2(2 \pm \beta)}{(1 - \rho_1^{2\pm\beta})(R\Phi)^2}\Bigg[&\left(a^2 + \frac{2ad}{4 \pm \beta} + 2\left(\frac{d}{4 \pm \beta}\right)^2\right)(1 - \rho_1^{4\pm\beta})/(4 \pm \beta) \\ &+ b^2(1 - \rho_1^{8\pm\beta})/(8 \pm \beta) - d^2\rho_1^{4\pm\beta} \ln^2 \rho_1/(4 \pm \beta) \\ &+ 2d\left(\frac{d}{4 \pm \beta} + a\right)(\rho_1^{4\pm\beta} \ln \rho_1)/(4 \pm \beta) \pm e^2(\rho_1^{\mp\beta} - 1)/\beta \\ &-2b\left(a + \frac{d}{6 \pm \beta}\right)(1 - \rho_1^{6\pm\beta})/(6 \pm \beta) - 2bd\rho_1^{6\pm\beta} \ln \rho_1/(6 \pm \beta) \\ &+ e((a + d/2)(1 - \rho_1^2) + d\rho_1^2 \ln \rho_1 - b(1 - \rho_1^4)/2)\Bigg],\end{aligned} \tag{73}$$

$\beta \neq 2, 4, 6, 8$ for inner-wall accumulation

where

$$a = \left(2 - R\Phi + \frac{2\theta}{2 \pm \beta}\right)/(2 \pm \beta) \tag{74}$$

$$b = 2/(4 \pm \beta) \tag{75}$$

and

$$d = 2\theta/(2 \pm \beta) \tag{76}$$

The number e equals

$$e = b - a \tag{77}$$

when zones form near the inner ANNC wall and

$$e = \rho_1^{2+\beta}(b\rho_1^2 - a + d \ln \rho_1) \tag{78}$$

when they form near the outer wall. Equations (73)–(78) are not expressed succinctly, but the direct substitution of Eqs. (74)–(78) into Eq. (73) does not result in much simplification.

The evaluation of Eq. (73) from Eq. (72) involves extensive (but not difficult) calculations, and a margin for error clearly exists. The plausibility of Eq. (73), however, is suggested by several limiting cases. First, as $\beta \to 0$ ($\lambda \to \infty$), Eq. (73) approaches the same limit for both numbers e given above, as it must; that limit is

$$\underset{\beta \to 0}{\Psi} = [(1 + \rho_1^2)\{(1 + \rho_1^4)/24 + \rho_1^2/3 + \theta^2/8\} + \theta(5 + 32\rho_1^2 + 5\rho_1^4)/36$$

$$- \rho_1^4/\theta]/\Phi^2 \tag{79}$$

This equation also describes the $\lambda \to \infty$ behavior for the $n \neq 1$ case as well, because Ψ becomes independent of the radial force as $\lambda \to \infty$. (Incidentally, Eq. 79 would also apply to a nonretained chromatographic zone, if the channel were an ANNC.) Secondly, as $\rho_1 \to 0$, Ψ equals

$$\Psi_{\beta \to 0, \rho_1 \to 0} = 1/24 \tag{80}$$

and the function $\chi = \Psi R/(1 - \rho_1)^2$ also equals 1/24. This number is the expected result for a circular channel of diameter $2w$ (*15*), which the ANNC becomes as $\rho_1 \to 0$. Finally, as $\rho_1 \to 1$, the ANNC becomes an OPPC of width w, for which χ must equal 1/105 as $\beta \to 0$ (*11*). A few expansions are required to evaluate the $\rho_1 \to 1$ limit. If one defines

$$\rho_1 = 1 - y \tag{81}$$

then

$$\Phi = 2y^2/3 + \cdots \tag{82}$$

$$\Theta = -2 + 2y - y^2/3 + (y^4 + y^5)/90 + 37y^6/3780 + \cdots \tag{83}$$

and

$$\ln \rho_1 = -\left(y + \frac{y^2}{2} + \frac{y^3}{3} + \frac{y^4}{4} + \frac{y^5}{5} + \frac{y^6}{6} + \frac{y^7}{7}\right) + \cdots \tag{84}$$

Substituting Eqs. (81)–(84) into Eq. (79), one finds that the bracketed expression [] in the latter equation approaches

$$\lim_{\beta,y\to 0}[] = 4y^6/945 + \cdots \tag{85}$$

and the function χ, Eq. (24), approaches

$$\lim_{\beta\to 0,\rho_1\to 1} \chi = \lim_{\beta,y\to 0} \frac{[]}{\Phi^2(1-\rho_1)^2} = \frac{[]}{4y^6/9} = \frac{1}{105} \tag{86}$$

as expected.

One needs the appropriate expression for retention ratio R to calculate H from the above equations. This expression is (*9*)

$$R = \frac{2}{\Phi}\left(\frac{2\rho_1^2}{4 \pm \beta} + \frac{2(1-\rho_1^2)}{(1-\rho_1^{2\pm\beta})(4 \pm \beta)} + \frac{\theta}{2 \pm \beta}\right),$$

$$\beta \neq 2, 4 \text{ for inner-wall retention} \tag{87}$$

Equations (87) and (73)–(78) approach the following limits as $\beta\to\infty$ ($\lambda\to 0$)

$$R_{in} = -\frac{2}{\beta\Phi}(2\rho_1^2 + \theta); \qquad R_{out} = \frac{2}{\beta\Phi}(2 + \theta), \qquad \lambda \ll 1 \tag{88}$$

$$\Psi_{out} = \left(\frac{2}{\beta}\right)^2, \qquad \lambda \ll 1 \tag{89}$$

$$\Psi_{in} = \left(\frac{2\rho_1}{\beta}\right)^2, \qquad \lambda \ll 1 \tag{90}$$

Combining Eqs. (88)-(90) and Eq. (24), one finds that the χ function equals

$$\chi_{out} = -\frac{8\lambda^3(\ln \rho_1)^3}{\Phi(1-\rho_1)^2}(2+\theta), \qquad \lambda \ll 1 \tag{91}$$

$$\chi_{in} = \frac{8\lambda^3(\ln \rho_1)^3\rho_1^2}{\Phi(1-\rho_1)^2}(2\rho_1^2+\theta), \qquad \lambda \ll 1 \tag{92}$$

when $\lambda \ll 1$, where R_{in}, R_{out}, Ψ_{in}, Ψ_{out}, χ_{in}, and χ_{out} are interpreted as before. The limit of Eqs. (91) and (92), as $\rho_1 \to 1$, is $24\lambda^3$, in agreement with Eq. (1).

Several singularities exist in Eqs. (73)-(78) and (87) for the relatively large β values, $\beta = 2$, 4, 6, and 8, when zones are retained near the inner wall. Additional equations could be developed to account for these singularities, as was done for retention ratio R (*9*). Because these β's will generally correspond to R values very near unity, however, the additional (extensive) work required does not seem justified. If a plate height corresponding to one of these β's were ever required, it could be simply estimated by interpolating between two H values, one calculated from a β slightly larger than, and the other calculated from a β slightly smaller than, the singularity in question.

All computations were carried out on the IBM 3081 GX computer at Southern Illinois University.

RESULTS AND DISCUSSION

Equations (53), (54), (91), and (92) can be written in the general form

$$\chi = \lambda^3 g(\rho_1, n) \tag{93}$$

where two functions $g(\rho_1,n)$ exist, one for inner-wall and one for outer-wall retention. Taking the common logarithm of both sides of Eq. (93), one obtains

$$\log \chi = 3 \log \lambda + \log g(\rho_1, n) \tag{94}$$

Thus, a plot of $\log \chi$ vs $\log \lambda$, in the λ range over which these equations apply, is a straight line of slope 3 and intercept $\log g(\rho_1,n)$.

Figures 2-5 are plots of $\log \chi$ vs $\log \lambda$ for the n values 5, 3, -1, and 1,

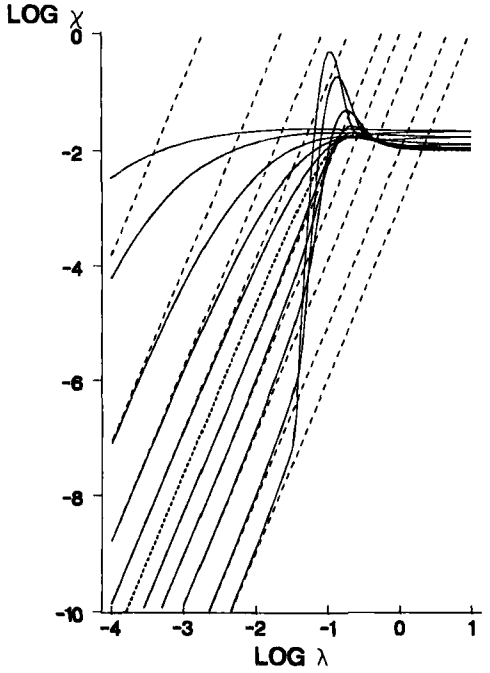

FIG. 2. Plot of log χ vs log λ for $n = 5$ (e.g., shear FFF). For $\lambda \ll 1$, the χ functions are, from top to bottom: χ_{out}, for $\rho_1 = 0.1, 0.2, 0.4, 0.6, 0.8$; χ_p (the central dashed curve); and χ_{in}, for $\rho_1 = 0.8, 0.6, 0.4, 0.2$, and 0.1.

and the ρ_1 values 0.8, 0.6, 0.4, 0.2, and 0.1. The bold dashed curve in the center of each figure is χ_p, which corresponds to $\rho_1 = 1$. The solid curves in Figs. 2–4 were computed numerically from Eqs. (46) and (51) with Simpson's rule. (Some scaling of the integrals was required to prevent numerical underflow and overflow.) The dashed lines in Figs. 2–4 were evaluated from the analytical approximations, Eqs. (53) and (54). The solid curves in Fig. 5 were calculated from Eqs. (73)–(78) and (87); the dashed lines were determined from the approximations, Eqs. (91) and (92). The approximations are best when $\lambda \ll 1$ and $\rho_1 \approx 1$ (i.e., when $|\alpha|$ and $\beta \gg 1$).

Several trends can be deduced from Figs. 2–5. When $\lambda \ll 1$, $\chi_{in} < \chi_p$ and $\chi_{out} > \chi_p$ when n is positive, but $\chi_{in} > \chi_p$ and $\chi_{out} < \chi_p$ when n is negative. Furthermore, the differences between χ_{in} and χ_p, and χ_{out} and χ_p, increase

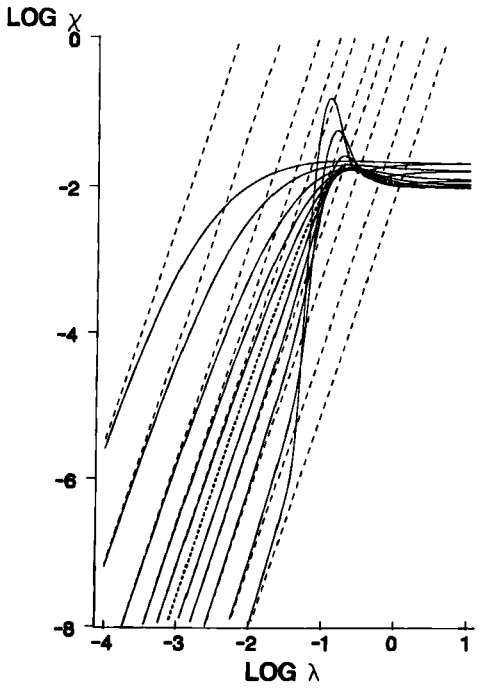

FIG. 3. Plot of log χ vs log λ for $n = 3$ (e.g., dielectrophoretic and magnetophoretic FFF). Otherwise, same as Fig. 2.

with decreasing ρ_1 and increasing $|n|$. These trends are comparable to those deduced from similar plots of retention ratio R vs λ (*9*). In addition, as $\lambda \to \infty$ and $R \to 1$, the functions χ_{in} and χ_{out} both approach the limiting χ value predicted by Eqs. (24) and (79).

The dependence of χ on λ can be simply rationalized when $\lambda \ll 1$. The random-walk model of nonequilibrium dispersion predicts that the zone variance σ^2 of well-retained FFF zones is proportional to the product of two terms: the time required for diffusive exchange among streamlines, which varies as the square of the zone thickness, and the zone velocity, which varies linearly with this thickness (*18*). Thus, H and χ vary with the cubic power of the zone thickness when $\lambda \ll 1$. Furthermore, since the zone thickness varies inversely with the local force near the accumulation wall, which itself varies inversely with λ, χ varies as the cubic power of λ, as confirmed by Eqs. (1), (53), (54), (91), and (92) when $\lambda \ll 1$.

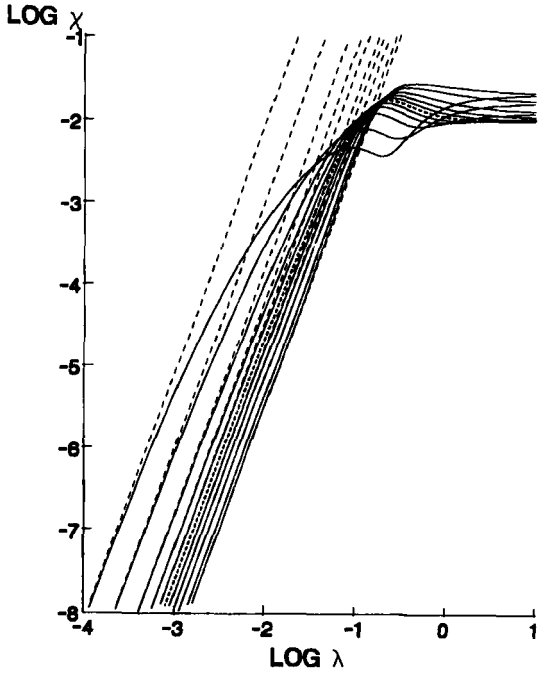

FIG. 4. Plot of log χ vs log λ for $n = -1$ (e.g., sedimentation FFF). For $\lambda \ll 1$, the χ functions are, from top to bottom: χ_{in}, for $\rho_1 = 0.1, 0.2, 0.4, 0.6, 0.8$; χ_p (the central dashed curve); and χ_{out}, for $\rho_1 = 0.8, 0.6, 0.4, 0.2$, and 0.1.

The thickness of zones in both OPPCs and ANNCs decreases as the force strength near the accumulation wall increases. At constant λ, the radial force F, Eq. (4), is larger near the inner wall and smaller near the outer wall of the ANNC than the uniform force F_p in the OPPC when n is positive. The force strengths are reversed when n is negative. Furthermore, the differences between F and F_p near the accumulation wall increase as ρ_1 decreases. When $\lambda \ll 1$, the force strength in the immediate vicinity of the accumulation wall principally determines the zone thickness. As argued above, the values of the χ functions are determined by this zone thickness and, consequently, by these local force strengths when $\lambda \ll 1$.

As $\lambda \to \infty$, the behavior of the χ functions cannot be justified by the explanation given above, because the bulk of the zone is not localized

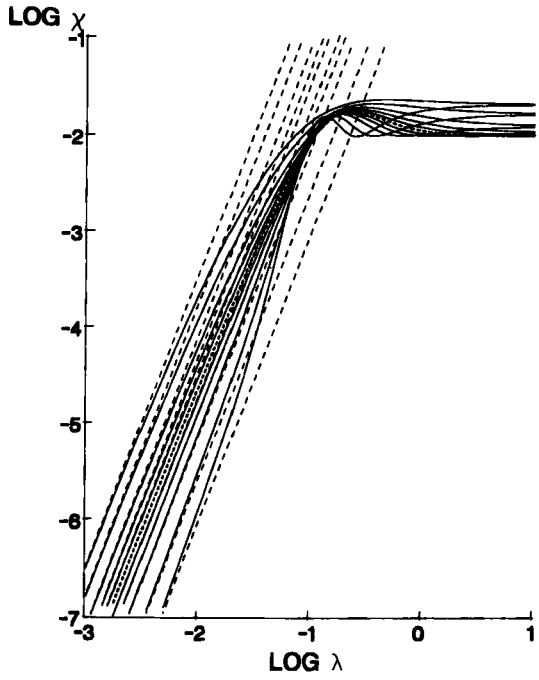

FIG. 5. Plot of log χ vs log λ for $n = 1$ (e.g., thermal, flow, and electrical FFF). Otherwise, same as Fig. 2.

near the accumulation wall. For example, the χ's in Figs. 2–5 exhibit local maxima near $\lambda \approx 0.1$; the maxima are most pronounced when n is large and positive and $\rho_1 \ll 1$. As λ is further increased, the functions χ_{out} and χ_p monotonically decrease to constant values. The function χ_{in}, however, either monotonically decreases to a constant value, or first decreases, then passes through a minimum, and finally monotonically increases to a constant value. The latter behavior is most pronounced for small ρ_1 and small, especially negative, n.

When $\lambda \ll 1$, the behavior of χ is largely governed by the magnitude of force F near the accumulation wall. The variation of the carrier velocity across gap w increasingly dictates the behavior of χ as λ is increased. As λ is increased, a large fraction of the zone eventually relaxes into the channel midsection near the maximum carrier velocity. Here, the streamline velocities are similar and do not strongly vary, as they do near the

accumulation walls. The similarity of the streamline velocities outweighs the increase in zone thickness, and χ decreases slightly, consequently passing through a maximum.

The large maxima in χ_{in} are observed when $\rho_1 \ll 1$ principally because, as ρ_1 decreases, $dV_z/d\rho$ increases very near the inner wall, and the maximum carrier velocity shifts toward the inner wall. (A plot of $V_z/\langle V_z \rangle$ vs channel width w for various ρ_1's is given in Ref. *9*.) When $\rho_1 \ll 1$, χ_{in} increases rapidly with increasing λ because the streamline velocities very near the inner wall vary significantly. The increase is largest for large positive n because the zone bulk is localized in this inner-wall region. As λ is further increased, the zone relaxes away from the wall; only a small relaxation is required, when $\rho_1 \ll 1$, for the zone bulk to be entrained by streamlines with similar velocities near the carrier maximum. The result is a rapid decrease in χ_{in}. The minima in χ_{in} are observed, possibly because in these cases the zone is principally localized near the velocity maximum. This explanation seems more plausible for small, rather than large, positive n and most plausible for negative n, because in this case the zone concentration is actually higher in the maximum velocity region than near the inner ANNC wall. The minima are indeed most pronounced for negative n.

A comparison of Figs. 2–5 to similar plots of log R vs log λ in Ref. *9* shows that, at constant λ and ρ_1, the departure of H from H_p is much greater than the departure of R from R_p. This behavior is observed (at least for small λ) because R depends on the first power of the characteristic zone thickness, whereas H depends, as observed above, on the third power of this thickness.

In general, the ANNC offers definite advantages over the OPPC when $R < R_p$ and $H < H_p$. Most significantly, the peak capacity of the ANNC is greater than that of the OPPC under these conditions, and multicomponent mixtures may be more efficiently resolved. Based on this study, and the previous one on the retention ratio R, one can conclude that R and especially H favorably depart from their parallel-plate counterparts when n is large, ρ_1 is small, and zones form near the inner ANNC wall, for $n > 0$, and near the outer wall, for $n < 0$. The differences can be exploited by decreasing ρ_1 to small values, although some shortcomings exist when $\rho_1 \ll 1$ (*9*). The advantage is perhaps most significant for shear FFF ($n = 5$) because the shear force always focuses components near the inner ANNC wall where R and H are pronouncedly less than R_p and H_p. Little advantage is expected for dielectrical FFF ($n = 3$), however, because pearl-chain formation is expected to limit extensively inner-wall retention (*19*). Magnetic FFF ($n = 3$) is likely to be subject to the same

limitation, although this subject has not been eamined in detail. Smaller advantages are anticipated for electrical, thermal, and flow FFF ($n = 1$) and sedimentation FFF ($n = -1$), but such advantages are realizable by judicious design of the ANNC and control over the experimental conditions.

GLOSSARY

a	$(2 - R\Phi + 2\theta/(2 \pm \beta))/(2 \pm \beta)$
A	coefficient indicating magnitude and direction of force F
ANNC	annular channel
b	$2/(4 \pm \beta)$
c	concentration
c^*	quasi-equilibrium concentration
d	$2\theta/(2 \pm \beta)$
D	diffusion coefficient
D	effective diffusion coefficient defined by Eq. (16)
e	Eq. (77) for inner-wall retention, and Eq. (78) for outer-wall retention
f	friction coefficient, kT/D
F	radial force, A/r^n
F_p	constant force in OPPC
g_1	value of ϕ at $\rho = \delta$
H	nonequilibrium plate height of zones in ANNCs
H_p	nonequilibrium plate height of zones in OPPCs
k	Boltzmann's constant
l	zone thickness in OPPCs
L	average distance of zone migration
n	power to which r is raised in equation for force F
N_r	one-dimensional radial flux
N_z	one-dimensional axial flux
OPPC	open parallel-plate channel
r	radial coordinate
r_1	inner radius of ANNC
r_2	outer radius of ANNC
R	retention ratio of zones in ANNCs
R_{in}	R for inner-wall retention
R_{out}	R for outer-wall retention
R_p	retention ratio of zones in OPPCs
t	time

T	absolute temperature
V_r	radial velocity of zone constituents induced by force F
V_z	axial velocity of carrier fluid
$\langle V_z \rangle$	average velocity of carrier fluid
w	channel width
W	work required to carry zone constituents across gap w
x	$\alpha\rho^{1-n}$
z	axial coordinate
α	$1/(\lambda(\rho_1^{1-n} - 1))$
β	$-(\lambda \ln \rho_1)^{-1}$
δ	lower integration limit of Ψ integral
δ'	δ value, expressed in terms of variable x
ε	fractional departure of c from c^*
θ	$(1 - \rho_1^2)/\ln \rho_1$
λ	$kT/\lvert W \rvert$
μ	reduced velocity, V_z/ν
ν	average zone velocity
ρ	reduced radial coordinate, r/r_2
ρ_1	r_1/r_2
σ^2	that fraction of the total zone variance originating from differential axial flow
ϕ	function of ε on which Ψ depends
Φ	$1 + \rho_1^2 + \theta$
χ	nonequilibrium coefficient in equation, $H = \chi w^2 \langle V_z \rangle / D$
χ_{in}	χ coefficient for inner-wall retention
χ_{out}	χ coefficient for outer-wall retention
χ_p	χ coefficient for parallel-plate channel
Ψ	nonequilibrium coefficient in equation, $H = \Psi r_2^2 \nu / D$
Ψ_{in}	Ψ coefficient for inner-wall retention
Ψ_{out}	Ψ coefficient for outer-wall retention
Ψ_p	Ψ coefficient for parallel-plate channel

Acknowledgment

The author thanks Southern Illinois University for the start-up funds with which this research was conducted.

REFERENCES

1. J. C. Giddings, *Sep. Sci. Technol., 19,* 831 (1984).
2. J. C. Giddings, *Anal. Chem., 53,* 1170A (1981).

3. H.-L. Lee, J. F. G. Reis, J. Dohner, and E. N. Lightfoot, *AIChE J., 20,* 776 (1974).
4. J. F. G. Reis and E. N. Lightfoot, *Ibid., 22,* 779 (1976).
5. A. S. Chiang, E. H. Kmiotek, S. M. Langan, P. T. Noble, J. F. G. Reis, and E. N. Lightfoot, *Sep. Sci. Technol., 14,* 453 (1979).
6. A. B. Shah, J. F. G. Reis, E. N. Lightfoot, and R. E. Moore, *Ibid., 14,* 475 (1979).
7. E. N. Lightfoot, P. T. Noble, A. S. Chiang, and T. A. Ugulini, *Ibid., 16,* 619 (1981).
8. J. M. Davis, F.-R. F. Fan, and A. J. Bard, *Anal. Chem., 59,* 1339 (1987).
9. J. M. Davis and J. C. Giddings, *J. Phys. Chem., 89,* 3398 (1985).
10. M. E. Hovingh, G. H. Thompson, and J. C. Giddings, *Anal. Chem., 42,* 195 (1970).
11. J. C. Giddings, Y. H. Yoon, K. D. Caldwell, M. N. Myers, and M. E. Hovingh, *Sep. Sci., 10,* 447 (1975).
12. J. F. G. Reis, D. Ramkrishna, and E. N. Lightfoot, *AIChE J., 24,* 679 (1978).
13. J. C. Giddings, *J. Chem. Phys., 49,* 81 (1968).
14. R. B. Bird, W. E. Stewart, and E. N. Lightfoot, *Transport Phenomena,* Wiley, New York, 1960.
15. J. C. Giddings, *Dynamics of Chromatography,* Dekker, New York, 1965.
16. J. M. Davis and J. C. Giddings, *Sep. Sci. Technol., 20,* 699 (1985).
17. J. C. Giddings, *J. Chromatogr., 4,* 11 (1960).
18. J. C. Giddings, *J. Chem. Educ., 50,* 667 (1973).
19. J. M. Davis and J. C. Giddings, *Sep. Sci. Technol., 21,* 969 (1986).

Received by editor February 8, 1988
Revised May 3, 1988